PLOS BIOLOGY

RESEARCH ARTICLE

QTL mapping of natural variation reveals that the developmental regulator *bruno* reduces tolerance to *P*-element transposition in the *Drosophila* female germline

Erin S. Kelleher[1]*, Jaweria Jaweria[1], Uchechukwu Akoma[1,2], Lily Ortega[1], Wenpei Tang[1]

1 Department of Biology and Biochemistry, University of Houston, Houston, Texas, United State of America, **2** Department of Molecular Physiology and Biophysics, Baylor College of Medicine, Houston, Texas, United States of America

* eskelleher@uh.edu

Citation: Kelleher ES, Jaweria J, Akoma U, Ortega L, Tang W (2018) QTL mapping of natural variation reveals that the developmental regulator *bruno* reduces tolerance to *P*-element transposition in the *Drosophila* female germline. PLoS Biol 16(10): e2006040. https://doi.org/10.1371/journal.pbio.2006040

Academic Editor: Harmit Malik, Fred Hutchinson Cancer Research Center, United States of America

Received: March 19, 2018

Accepted: September 26, 2018

Published: October 30, 2018

Data Availability Statement: All relevant data are within the paper and its Supporting Information files.

Funding: National Science Foundation www.nsf.gov (grant number 1457800). ESK. The funder had no role in study design, data collection and analysis, decision to publish, or preparation of the manuscript.

Competing interests: The authors have declared that no competing interests exist.

Abstract

Transposable elements (TEs) are obligate genetic parasites that propagate in host genomes by replicating in germline nuclei, thereby ensuring transmission to offspring. This selfish replication not only produces deleterious mutations—in extreme cases, TE mobilization induces genotoxic stress that prohibits the production of viable gametes. Host genomes could reduce these fitness effects in two ways: resistance and tolerance. Resistance to TE propagation is enacted by germline-specific small-RNA-mediated silencing pathways, such as the Piwi-interacting RNA (piRNA) pathway, and is studied extensively. However, it remains entirely unknown whether host genomes may also evolve tolerance by desensitizing gametogenesis to the harmful effects of TEs. In part, the absence of research on tolerance reflects a lack of opportunity, as small-RNA-mediated silencing evolves rapidly after a new TE invades, thereby masking existing variation in tolerance. We have exploited the recent historical invasion of the *Drosophila melanogaster* genome by *P*-element DNA transposons in order to study tolerance of TE activity. In the absence of piRNA-mediated silencing, the genotoxic stress imposed by *P*-elements disrupts oogenesis and, in extreme cases, leads to atrophied ovaries that completely lack germline cells. By performing quantitative trait locus (QTL) mapping on a panel of recombinant inbred lines (RILs) that lack piRNA-mediated silencing of *P*-elements, we uncovered multiple QTL that are associated with differences in tolerance of oogenesis to *P*-element transposition. We localized the most significant QTL to a small 230-kb euchromatic region, with the logarithm of the odds (LOD) peak occurring in the *bruno* locus, which codes for a critical and well-studied developmental regulator of oogenesis. Genetic, cytological, and expression analyses suggest that *bruno* dosage modulates germline stem cell (GSC) loss in the presence of *P*-element activity. Our observations reveal segregating variation in TE tolerance for the first time, and implicate gametogenic regulators as a source of tolerant variants in natural populations.

Abbreviations: Δ2-LOD CIs, Δ2-LOD drop confidence intervals; 3L, chromosome 3L; *bru1*, *bruno*; *bru2*, *bruno-2*; CB, cystoblast; *crok*, *crooked*; *CyO*, *Curly-O*; *Df(3R)osk*, deficiency on chromosome 3R over *oskar*; dm6, *Drosophila melanogaster* reference assembly; DSB, double-stranded break; DSPR, *Drosophila* Synthetic Population Resource; DV, dorsoventral; F1, filial 1; F2, filial 2; GSC, germline stem cell; Hts-1B1, hu li tai shao; KRAB-ZFP, Kruppel-associated box zinc-finger protein; LOD, logarithm of the odds; p53, tumor protein 53; piRNA, Piwi-interacting RNA; QTL, quantitative trait locus; *rho-6*, *rhomboid 6*; RIL, recombinant inbred line; SNP, single nucleotide polymorphism; TE, transposable element; *ThrRS*, *Threonyl-tRNA synthetase*; *TM2*, third marked 2; *TM3*, third marked 3.

Author summary

Transposable elements (TEs), or "jumping genes," are mobile fragments of selfish DNA that leave deleterious mutations and DNA damage in their wake as they spread through host genomes. Their harmful effects are known to select for resistance by the host, in which the propagation of TEs is regulated and reduced. Here, we study for the first time whether host cells might also exhibit tolerance to TEs, by reducing their harmful effects without directly controlling their movement. By taking advantage of a panel of wild-type *Drosophila melanogaster* that lack resistance to *P*-element DNA transposons, we identified a small region of the genome that influences tolerance of *P*-element activity. We further demonstrate that a gene within that region, *bruno*, strongly influences the negative effects of *P*-element mobilization on the fly. When *bruno* dosage is reduced, the fertility of females carrying mobile *P*-elements is enhanced. The *bruno* locus encodes a protein with no known role in TE regulation but multiple well-characterized functions in oogenesis. We propose that *bruno* function reduces tolerance of the developing oocyte to DNA damage that is caused by *P*-elements.

Introduction

Transposable elements (TEs) are omnipresent and abundant constituents of eukaryotic genomes, comprising up to 80% of genomic DNA in some lineages (reviewed in [1]). The evolutionary footprint of TEs is extensive, including dramatic genome size expansions [2,3], acquisition of new regulatory networks [4,5], structural mutations [6], novel genes [7–9], and adaptive insertions [10–12]. However, the charismatic and occasionally beneficial impact of TEs over evolutionary time masks their fundamental identity as intragenomic parasites and mutagens. In addition to causing deleterious mutations [13,14], TEs can exert lethal, genotoxic effects on host cells by producing abundant double-stranded breaks (DSBs) during insertion and excision [15,16]. TEs are therefore intragenomic parasites.

Host developmental and evolutionary responses to parasites, pathogens, and herbivores are broadly delineated into two categories: resistance and tolerance (reviewed in [17,18]). Mechanisms of resistance prevent—or limit the spread of—infection or herbivory. By contrast, mechanisms of tolerance do not affect propagation but rather limit the fitness costs to the host. With respect to TEs, resistance by eukaryotic genomes is enacted by small-RNA-mediated silencing pathways [19] and Kruppel-associated box zinc-finger proteins (KRAB-ZFPs)[20], which regulate the transcription and subsequent transposition of endogenous TEs. However, it remains unknown whether genomes can also evolve tolerance of TEs by altering how host cells are affected by TE activity. Tolerance therefore represents a wholly unexplored arena of the evolutionary dynamics between TEs and their hosts. Germline tolerance of TEs is predicted to be of particular importance because of the significance of this cell lineage in ensuring the vertical transmission of the parasite and the reproductive fitness of the host.

The absence of research on tolerance is at least partially due to the primacy of resistance: endogenous TEs are overwhelmingly repressed by host factors in both germline and somatic tissues [19,21,22]. However, the invasion of the host genome by a novel TE family, which happens recurrently over evolutionary timescales (reviewed in [23]), provides a window of opportunity through which tolerance could be viewed, both empirically and by natural selection. The absence of evolved resistance in the host against a new invader could reveal differential responses of germline cells to unrestricted transposition. A classic example of genome invasion by a novel TE is provided by *P*-elements, DNA transposons that have recently colonized two

Drosophila species. *P*-elements first appeared in genomes of *D. melanogaster* around 1950 (reviewed in [24]) and later colonized its sister species *D. simulans* around 2006 [25,26]. Particularly for *D. melanogaster*, a large number of naïve strains collected prior to *P*-element invasion are preserved in stock centers and laboratories, providing a potential record of ancestral genetic variation in tolerance [27,28]. Furthermore, 15 of these naïve strains were recently used to develop the *Drosophila* Synthetic Population Resource (DSPR), a panel of highly recombinant inbred lines (RILs) that serve as a powerful tool kit for discovering the natural genetic variants influencing quantitative traits [29–31].

Here, we harness the mapping power of the DSPR to screen for phenotypic and genetic variation in the tolerance of the *D. melanogaster* female germline to unrestricted *P*-element activity. We developed a novel screen for phenotypic variation in host tolerance by taking advantage of the classic genetic phenomenon of hybrid dysgenesis, in which TE families that are inherited exclusively paternally can induce a sterility syndrome in offspring because of an absence of complementary maternally transmitted regulatory small RNAs (Piwi-interacting RNA [piRNAs], reviewed in [24,32,33]). The dysgenesis syndrome induced by *P*-elements in the female germline is particularly severe and can be associated with a complete loss of germline cells [15,34,35]. *P*-element hybrid dysgenesis is directly related to genotoxic stress, as apoptosis is observed in early oogenesis in dysgenic females [15], and the DNA damage response factors *checkpoint kinase 2* and *tumor protein 53* (*p53*) act as genetic modifiers of germline loss [35]. Variation in the sensitivity of the DNA damage response to DSBs therefore represents one potential cellular mechanism for tolerance.

By phenotyping the germline development of >32,000 dysgenic female offspring of RIL mothers, we uncovered substantial heritable variation in female germline tolerance of *P*-element activity. We furthermore mapped this variation to a small 230-kb quantitative trait locus (QTL) on the second chromosome and associated it with the differential expression of *bruno*, a well-studied developmental regulator of oogenesis with no known function in TE repression or DNA damage response [36–39]. We further demonstrate that *bruno* loss-of-function alleles act as dominant suppressors of germline loss, and relate these effects to the retention of germline stem cells (GSCs) in dysgenic females. Our findings represent the first demonstration of natural variation in TE tolerance in any organism. They further implicate regulators of gametogenesis, such as *bruno*, as a source of tolerant variants that could be beneficial when new TEs invade the host.

Results

Maternal genotype, but not zygotic age, is a strong predictor of dysgenic F1 atrophy

We first sought to uncover phenotypic variation in germline tolerance of *P*-element activity among a panel of highly recombinant RILs derived from eight founder genomes [29]. To quantify tolerance, we performed dysgenic crosses between RIL females and males from the *P*-element containing strain Harwich (Fig 1A). Harwich is a strong paternal inducer of hybrid dysgenesis, producing filial 1 (F1) females with 100% atrophied ovaries in crosses with naïve females at the restrictive temperature of 29 ˚C [28]. We therefore performed our crosses at 25 ˚C, a partially permissive temperature at which intermediate levels of ovarian atrophy are observed [40,41]. Because *P*-element dysgenic females may recover their fertility as they age, through zygotic production of *P*-element–derived piRNAs [42], we assayed both 3-day-old and 21-day-old F1 female offspring from each RIL. In total, we documented the incidence of atrophied ovaries among 17,150 3-day-old and 15,039 21-day-old F1 female offspring, and estimated the proportion of F1 atrophy within broods of ≥20 3-day-old and 21-day-old

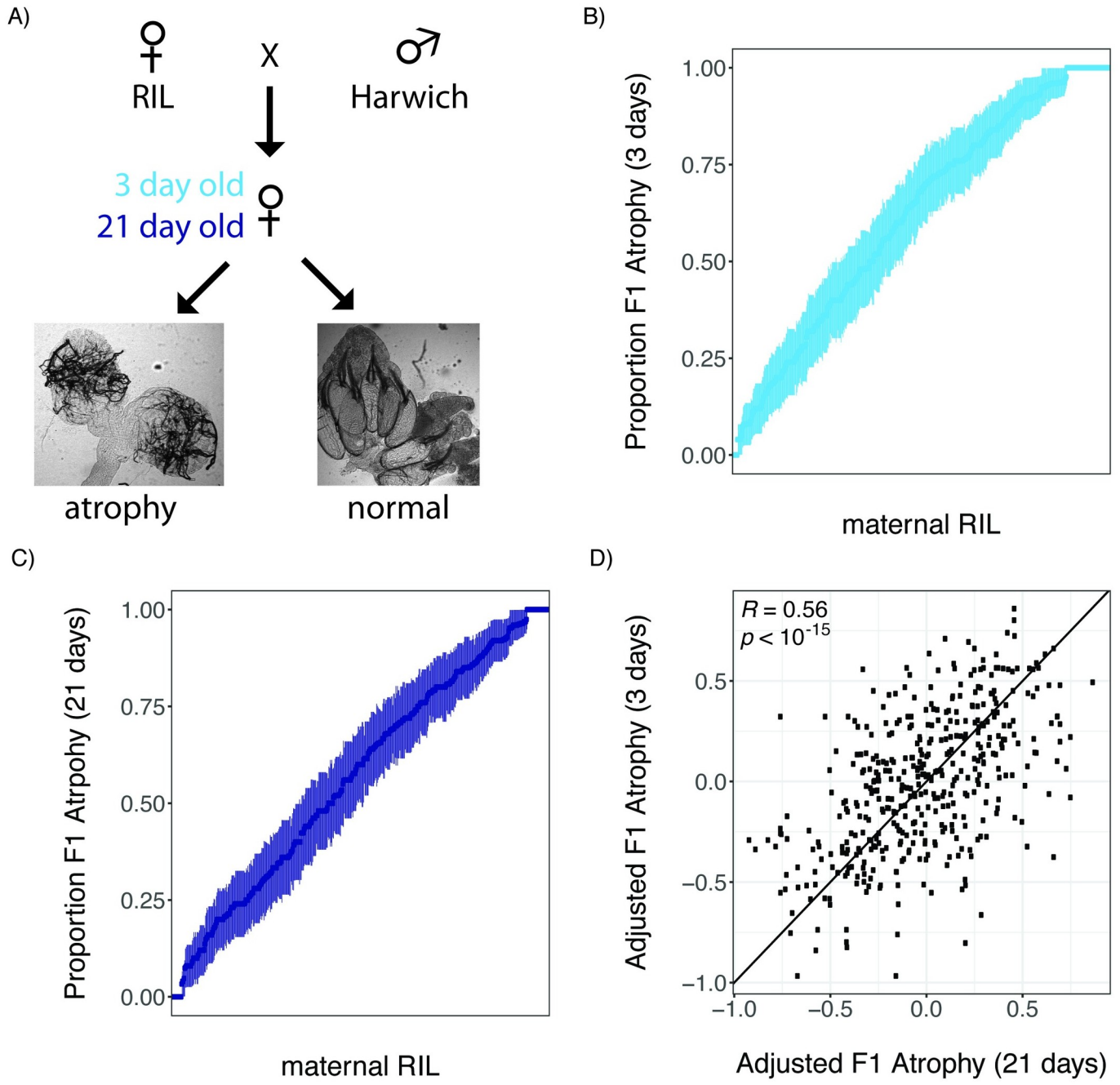

Fig 1. Heritable phenotypic variation in tolerance of *P*-element activity in the female germline. (A) Crossing scheme for documenting variation in tolerance of *P*-element activity among RIL offspring, including representative images of atrophied and normal ovaries. (B and C) Phenotypic variation in the proportion of 3-day-old (B) and 21-day-old (C) F1 female offspring of different RILs. RILs are sorted according to the proportion of F1 atrophy observed in their offspring, and error bars indicate the standard error of the estimated proportion. (D) Scatterplot of the arsine-transformed proportion of F1 atrophy observed among 3-day-old and 21-day-old offspring of the same line, after accounting for the effects of experimenter and experimental block. The individual numerical values for panels B, C, and D can be found in S1, S2 and S3 Data, respectively. F1, filial 1; RIL, recombinant inbred line.

https://doi.org/10.1371/journal.pbio.2006040.g001

offspring from 592 and 492 RILs, respectively (Fig 1B and 1C). Notably, because we phenotyped F1 offspring, our phenotypic variation will be determined only by variants in which one of the RIL alleles is at least partially dominant to the Harwich allele, or maternal effects that reflect only the RIL genotype.

We observed continuous variation in the proportion of F1 atrophy among broods of both 3-day-old and 21-day-old offspring of different RIL genotypes, capturing the full range of proportional values from 0 to 1 (Fig 1B and 1C). After accounting for the effects of experimenter and experimental block, the incidence of ovarian atrophy is strongly correlated among 427 RILs for which we sampled broods of both 3-day-old and 21-day-old F1 females (Pearson's $R = 0.56$, $p > 10^{-15}$, Fig 1D). Because broods of different age classes were sampled from separate crosses and experimental blocks, this correlation strongly implies that phenotypic differences are explained by the maternal genotype. Indeed, based on the F1 atrophy proportions measured in broods of different ages, we estimate that the broad sense heritability of F1 ovarian atrophy among the RIL offspring was 40.35% (see Materials and methods). Furthermore, we saw greater reproducibility across a small sample of 14 RILs, for which we phenotyped two independent 21-day broods (Pearson's $R = 0.97$, $p > 10^{-8}$), suggesting even higher heritability among offspring of the same age class.

Despite the previous observation of developmental recovery from hybrid dysgenesis [42], the relationship between age and the proportion of F1 atrophy is only marginally significant in our data ($F_{1,1037} = 3.57$, $p = 0.058$). Furthermore, 21-day-old dysgenic females exhibited only a 0.63% decrease in the proportion of F1 atrophy when compared to 3-day-old females, indicating that the overall effect of age in our crosses was very modest. Finally, we did not observe a group of RILs in which ovarian atrophy is much more common among 3-day-old as compared with 21-day-old F1 females (Fig 1D), as would be predicted if there were genetic variation for developmental recovery across the RIL panel. The absence of developmental recovery in our experiments could reflect differences in developmental temperature between our two studies (22 ˚C in [42] and 25 ˚C here). Alternatively, the causative variant that allows for developmental recovery could be absent from the founder RILs.

QTL mapping of dysgenic F1 atrophy

To identify the genomic regions that harbor causative genetic variation in tolerance, we performed a QTL analysis using the published RIL genotypes [29]. In these data, the founder allele (A1–A8) carried by each RIL is inferred probabilistically for 10-kb windows along the euchromatic regions of the major autosomes 2 and 3, and the X chromosome [29]. The fourth chromosome is ignored because the absence of recombination makes it uninformative for QTL mapping (reviewed in [43]).

Consistent with the strongly correlated phenotypes of 3-day-old and 21-day-old offspring (Fig 1D), we identified a single major effect QTL associated with phenotypic variation at both developmental time points (Fig 2A). Additionally, the Δ2-LOD drop confidence intervals (Δ2-LOD CIs) of the logarithm of the odds (LOD) peak from each analysis are both narrow (<300 kb) and highly overlapping (Table 1). The peak explains 14.2% and 14.8% of variation in ovarian atrophy among 3-day-old and 21-day-old F1 females, indicating it is a major determinant of heritable variation. Multiple minor peaks close to the centromere on chromosome 3 left (3L) may represent another source of heritable variation in 3-day-old females.

To further narrow the location of genetic variation in tolerance, we took advantage of the striking concordance in QTL mapping for the 3-day-old and 21-day-old data sets and performed a combined analysis, including all 660 RILs whose F1 offspring were sampled at either developmental time point. F1 female age was included as a covariate (see Materials and methods). From this analysis we obtained a final Δ2-LOD CI for the major QTL peak, which corresponds to a 230-kb genomic region containing 18 transcribed genes—15 protein-coding and 3 noncoding (Fig 2B). Simulation testing of the statistical properties of the DSPR indicates that a causative variant explaining 10% of phenotypic variation lies within

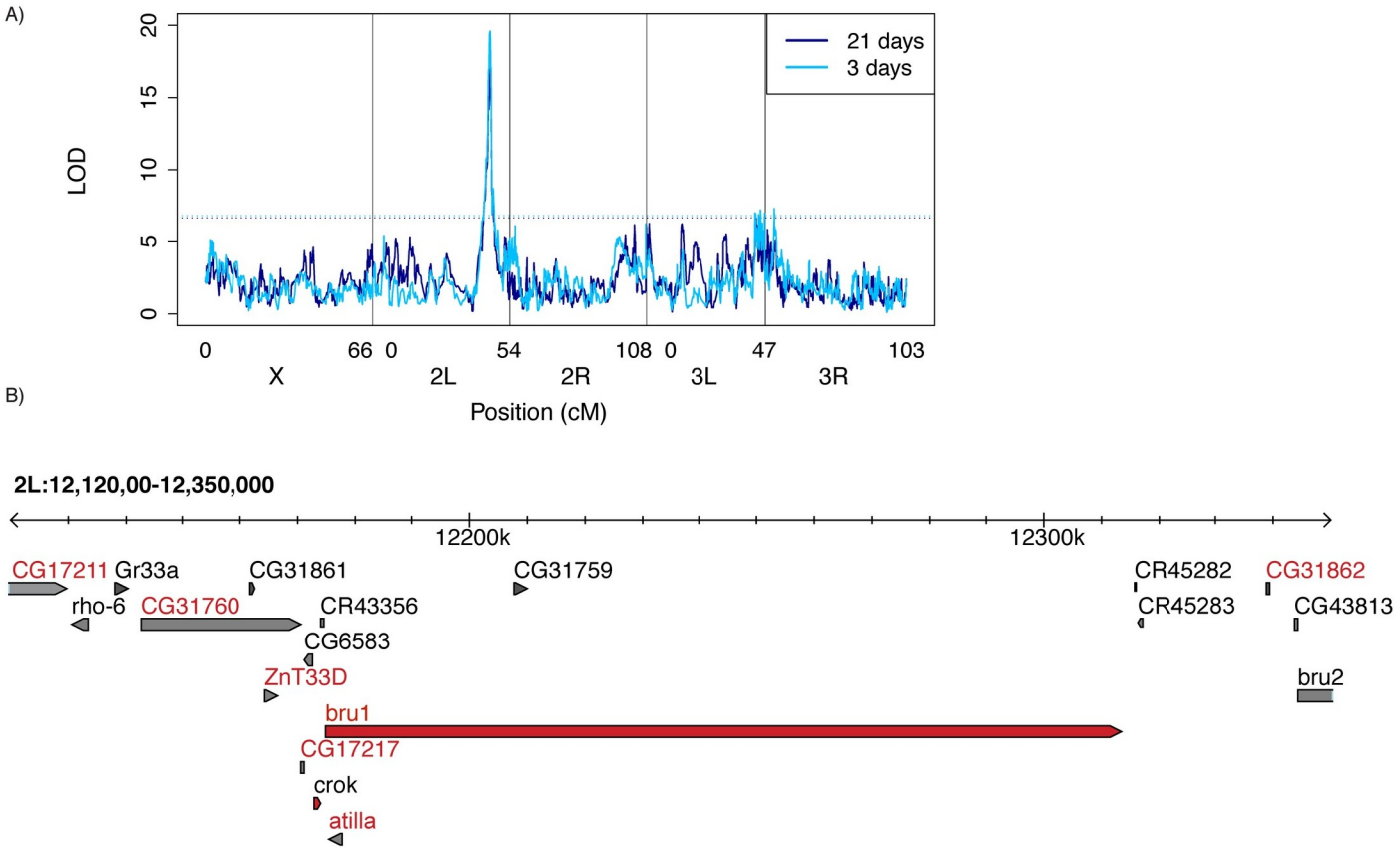

Fig 2. QTL mapping of variation in *P*-element tolerance. (A) LOD ratio of the observed association between maternal RIL genotype [29] and the adjusted proportion of F1 atrophy phenotype. Higher LOD scores correspond to stronger evidence of linkage, and significant LOD scores are above the threshold (dotted line), which was obtained from 1,000 permutations of the observed data. (B) Two LOD drop confidence interval of the QTL peak based on a combined QTL analysis including both 3-day-old and 21-day-old F1 females. Genes indicated by red letters are potentially affected by polymorphisms in the RIL founders that are in phase with the inferred allelic classes (Fig 3 [46]). Gene models indicated in red are highly expressed in the *Drosophila melanogaster* ovary [47]. The individual numerical values required to generate LOD plots for 3-day-old and 21-day-old F1 females can be found in S4 and S5 Data, respectively. *bru1*, *bruno*; *bru2*, *bruno-2*; cM, centimorgan; *crok*, *crooked*; F1, filial 1; LOD, logarithm of the odds; *P*-element; QTL, quantitative trait locus; *rho-6*, *rhomboid 6*; RIL, recombinant inbred line.

https://doi.org/10.1371/journal.pbio.2006040.g002

the Δ2-LOD drop CI 96% of time for sample sizes of 600 RILs [30]. Furthermore, overestimation of variance explained by a QTL (i.e., the Beavis effect) is rare in DSPR studies sampling greater than 500 RILs, particularly for variants explaining ≥10% of variation [48]. Therefore, given our sample (660 RILs) and effect (about 14%) sizes, the Δ2-LOD CI we infer for our

Table 1. QTL peak positions. The position of the major QTL peak for 3-day-old F1 females, 21-day-old F1 females, and the combined data set are shown. For each analysis, the peak position, Δ2-LOD drop confidence interval, and Bayesian credible interval [44] in dm6 [45] are provided. The percent of phenotypic variation explained by the QTL peak is based on the genotype of each sampled RIL at the LOD peak position. The individual numerical values required to identify LOD peaks and intervals for 3-day-old, 21-day-old, and both F1 females can be found in S4, S5 and S3 Data, respectively.

Data Set	LOD Score	Peak Position	Δ2-LOD CI	Bayes CI	Percent Variation
3-day-old females	19.59	2L:12,260,000	2L:12,080,000–12,380,000	2L:12,080,000–12,320,000	14.2
21-day-old females	17.22	2L:12,250,000	2L:12,110,000–12,390,000	2L:12,160,000–12,330,000	14.8
both	34.90	2L:12,260,000	2L:12,120,000–12,350,000	2L:12,180,000–12,310,000	13.8

Abbreviations: Δ2-LOD, Δ2 logarithm of the odds; CI, confidence interval; dm6, *Drosophila melanogaster* genome release 6; LOD, logarithm of the odds; QTL, quantitative trait locus; RIL, recombinant inbred line.

https://doi.org/10.1371/journal.pbio.2006040.t001

major peak should be conservative. Indeed, Bayesian credible intervals, an alternate approach for identifying QTL windows [44], are even narrower than those estimated by Δ2-LOD CI (Table 1).

Of the 18 genes within the QTL peak, only *bruno* and *crooked* are highly expressed in the *D. melanogster* ovary [47]. While *bruno* is a translational repressor whose major essential role is in oogenesis [37,49,50], *crooked* is a more broadly expressed component of septate junctions, which is essential for viability [51]. The LOD peak resides within the 138-kb *bruno* locus, which, in addition to its function, makes it the strongest candidate for the source of causative variation.

Two classes of tolerance alleles

We next sought to partition founder alleles at the QTL peak into phenotypic classes, in order to better understand the complexity of causative genetic variation. First, we identified all sampled RILs whose genotype was probabilistically assigned ($p > 0.95$) to a single founder (A1–A8) at the LOD peak, and estimated the phenotypic effect associated with each founder allele (Fig 3A and 3B). We then used stepwise regression (see Materials and methods) to identify the minimum number of allelic classes required to explain phenotypic variation associated with the founder alleles. For both age classes, we found strong evidence for two allelic classes, one sensitive and one tolerant, which were sufficient to explain phenotypic variation in tolerance. This implies that the major QTL peak could correspond to a single segregating genetic variant. Furthermore, with the exception of founder A8, founder alleles were assigned to the same allelic class for both age cohorts, revealing that allelic behavior is highly biologically reproducible.

To further study phenotypic differences between tolerant and sensitive alleles, we identified three pairs of background-matched RILs, which exhibited a tolerant (founder A4) or a sensitive (founder A5) haplotype across the QTL window but otherwise shared a maximal number of alleles from the same founder across the remainder of the genome. Consistent with our QTL mapping, these RIL pairs differed dramatically in the incidence of ovarian atrophy they displayed in crosses with Harwich males (Fig 4A). While we did not detect a significant effect of genetic background (drop in deviance = 3.57, df = 2, $p = 0.17$), the QTL haplotype was strongly associated with the incidence of ovarian atrophy (drop in deviance = 52.01, df = 1, $p = 5.36 \times 10^{-13}$). RILs carrying the tolerant haplotype exhibited 39% less F1 ovarian atrophy than those carrying the sensitive haplotype.

To determine whether reduced ovarian atrophy conferred by tolerant alleles increases female reproductive fitness, we examined the presence and number of filial 2 (F2) adults produced by young (0–5-day-old) F1 female offspring of tolerant and sensitive dysgenic crosses (Fig 4B). The proportion of F1 sterility was somewhat lower than the proportion of F1 atrophy for the same dysgenic cross (Fig 4A versus 4B), consistent with loss of germline cells in early adult stages. Equivalent to ovarian atrophy, there was no significant effect of genetic background (drop in deviance = 5.26, df = 2, $p = 0.07$), but the QTL haplotype was strongly associated with F1 sterility (drop in deviance = 65.787, df = 1, $p = 5.55 \times 10^{-16}$). F1 females carrying the tolerant haplotype exhibited a 54% reduction in sterility as compared with those carrying the sensitive haplotype. Interestingly, when we examine the number of F2 offspring produced by fertile F1 females from resistant and tolerant crosses (Fig 4C), we detect dramatic effects of genetic background ($F_{2,110} = 29.05$, $p = 7.48 \times 10^{-11}$) but no significant effect of the tolerant allele ($F_{1,110} = 1.01$, $p = 0.31$). Therefore, while tolerant alleles enhance female reproductive fitness by increasing the odds of fertility, other genetic factors likely determine the number of offspring produced by those fertile females.

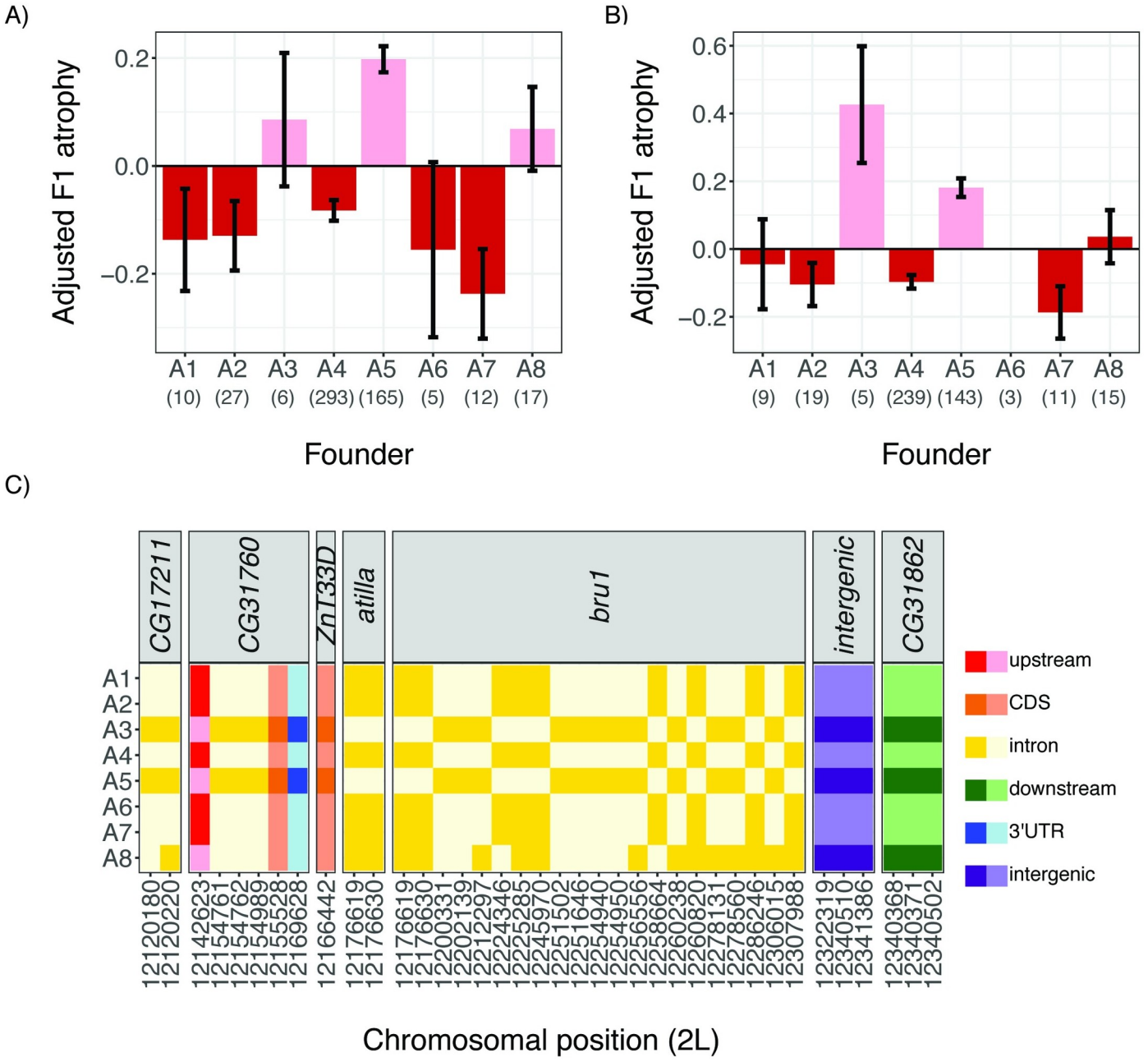

Fig 3. Phenotypic classes of founder alleles at the major QTL peak. The mean adjusted F1 atrophy among 3-day-old females (A) and 21-day-old females (B) is shown for RILs carrying each of the eight founder alleles. Error bars denote standard error. QTL phasing (see Materials and methods) detects two allelic classes for both the 3-day-old and 21-day-old phenotypes: a sensitive allele that increases the odds of F1 ovarian atrophy (pink) and a tolerant allele that decreases the odds of F1 ovarian atrophy (red). The assignment of founder alleles to phenotypic classes across ages is consistent for all founders except A8. (C) In-phase SNPs in Population A RIL founder genomes, indicated by their position in the *Drosophila melanogaster* reference assembly (dm6, [45]). SNPs are colored according to the function of the affected sequence, and shaded according to whether the founder exhibits the reference (light) or alternate (dark) allele. The individual numerical values required to generate bar plots for panels A and B can be found in S4 and S5 Data, respectively. In-phase polymorphisms represented in panel C are provided in S1 Table. *bru1*, *bruno* CDS, coding sequence; dm6, *Drosophila melanogaster* reference assembly; F1,filial 1; QTL, quantitative trait locus; RIL, recombinant inbred line; SNP, single nucleotide polymorphism.

https://doi.org/10.1371/journal.pbio.2006040.g003

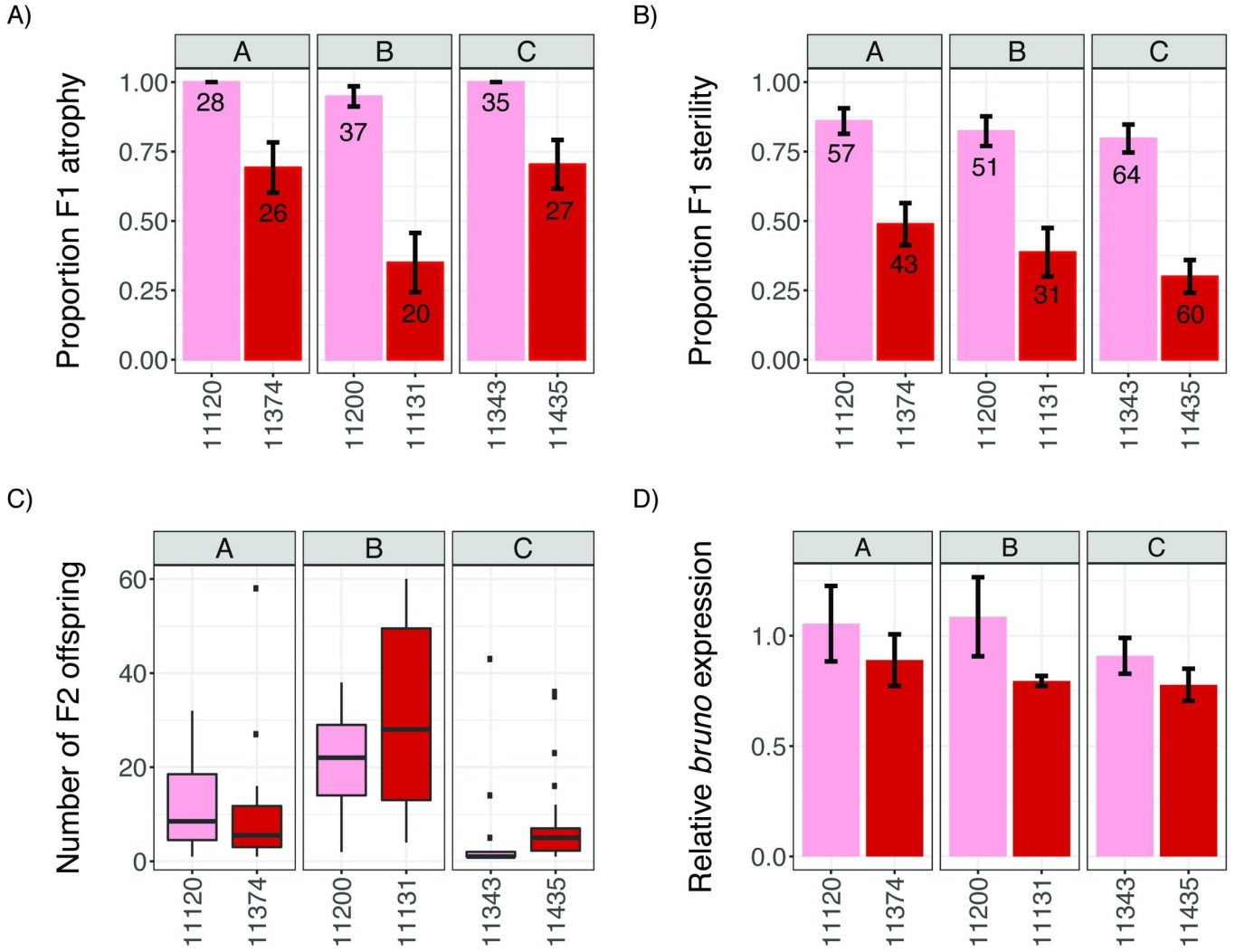

Fig 4. Tolerant alleles are associated with enhanced fertility and reduced *bruno* expression. Phenotypes of background-matched RILs (A, B, and C) carrying sensitive (A5, pink) and tolerant (A4, red) haplotypes across the QTL peak are compared. (A-B) Incidence of ovarian atrophy (A) and sterility (B) among dysgenic F1 female offspring of crosses between RIL females and Harwich males. Numbers in each bar indicate the sample size. (C) Offspring production of fertile F1 females from B. (D) Ovarian *bruno* expression relative to *rpl32* in each RIL. Error bars in A, B, and D indicate the standard error. The individual numerical values required to generate bar and box plots for panels A, B/C, and D can be found in S6, S7 and S8 Data, respectively. F1, filial 1; F2, filial 2; QTL, quantitative trait locus; RIL, recombinant inbred line.

https://doi.org/10.1371/journal.pbio.2006040.g004

Tolerant alleles are associated with reduced *bruno* expression

In light of the simple biallelic behavior of our phenotype, we sought to identify polymorphisms within the founder strains whose genotypic differences matched their phenotypic classifications (i.e., "in-phase" polymorphisms [29,31], Fig 3C). We excluded A8 from these analyses because of the ambiguity of its allelic class. In total, we identified 36 in-phase single nucleotide polymorphisms (SNPs), which potentially affect the function of only seven transcribed genes in the QTL interval ([46] S1 Table, Figs 2B and 3C). We did not identify any in-phase, segregating TE insertions, although a recent reassembly of the founder A4 genome based on long single-molecule real-time sequencing reads suggests many TE insertions remain unannotated [52]. Focusing on *bruno* and *crooked*, the two genes in the QTL window that are highly expressed in the ovary [47], 22 of the in-phase SNPs are within *bruno* introns, while none are

found in the gene body or upstream of *crooked*. Furthermore, none of the 36 in-phase SNPs are nonsynonymous, implying a regulatory difference between the tolerant and sensitive alleles.

To determine if tolerance is associated with *bruno* regulation, we compared ovarian expression of *bruno* in young (3-day-old) females from our background-matched RIL pairs carrying a tolerant or sensitive haplotype across the QTL locus. While we observed only modest effects of genetic background on *bruno* expression (likelihood ratio test = 6.57, df = 2, $p = 0.04$), we observed dramatic effects of founder haplotype at the QTL window (likelihood ratio test = 29.47, df = 1, $p = 5.67 \times 10^{-8}$). Across genetic backgrounds, tolerant alleles were associated with a 20% reduction in *bruno* expression (95% CI: 14%–26%), suggesting that *bruno* function reduces germline tolerance of *P*-element activity.

bruno is a strong dominant suppressor of *P*-element–induced ovarian atrophy

Given the differences in *bruno* expression between sensitive and tolerant alleles, we wondered whether *bruno* loss-of-function alleles affect the atrophy phenotype. For comparison, we also considered available alleles from three other ovary-expressed genes that are located within the Δ2-LOD CI of the 21-day-old or 3-day-old female analyses, but not in the combined analysis: *ced-12*, *Rab6*, and *Threonyl-tRNA synthetase* (*ThrRS*). We reasoned that, because the causative variant is almost certainly not recessive, being found only in the maternal RIL genotype, mutant alleles might also exhibit non-recessive effects. We therefore used balanced heterozygous females as mothers in dysgenic crosses with Harwich males and compared the incidence of F1 ovarian atrophy among their 3–7-day-old F1 females (*mutant*/+ versus *balancer*/+). Strikingly, while *ced-12*, *Rab6*, and *ThrRS* alleles had no effect on the incidence of ovarian atrophy (Fig 5A), two different *bruno* alleles ($bruno^{RM}$ and $bruno^{QB}$) acted as dominant suppressors (Fig 5B). In contrast to their balancer control siblings, who exhibited 64%–75% ovarian atrophy, $bruno^{RM}$/+ and $bruno^{QB}$/+ offspring exhibited only 13% and 20% atrophy, respectively—a dramatic reduction. We further observed that an independently derived *bruno* deficiency [53,54] suppresses ovarian atrophy to a similar degree (Fig 5B), indicating these effects cannot be attributed to a shared linked variant on the $bruno^{RM}$ and $bruno^{QB}$ chromosomes [49].

Notably, the non-recessive, fertility-enhancing effects of *bruno* loss-of-function alleles in dysgenic females contrasts with their effects on the fertility of non-dysgenic females, in which they act as recessive female steriles [49]. Our observations therefore suggest that a novel phenotype of *bruno* alleles is revealed by the dysgenic female germline. Furthermore, our observation that reduced *bruno* dosage suppresses ovarian atrophy is fully consistent with our observation that tolerant alleles are associated with reduced *bruno* expression (Fig 4D).

bruno's effects on ovarian atrophy are associated with GSC retention

bruno is a translational regulator with three known functions in *D. melanogaster* oogenesis. At the start of oogenesis in the ovarian substructure called the germaria, *bruno* is required to promote the differentiation of cystoblasts (CBs), the immediate daughters of GSCs [37,55]. In mid-oogenesis, Bruno protein blocks vitellogenesis if not properly sequestered by its mRNA target *oskar* [38,39]. Finally, in late oogenesis, Bruno repression of *oskar* translation is required to establish dorsoventral (DV) patterning in the subsequent embryo [36]. This final role of *bruno* affects only the morphology of egg chambers, but not their production, suggesting that it cannot account for *bruno*'s effects in dysgenic germlines. We therefore focused on *bruno*'s earlier roles in GSC differentiation and vitellogenesis, which are distinguishable by their

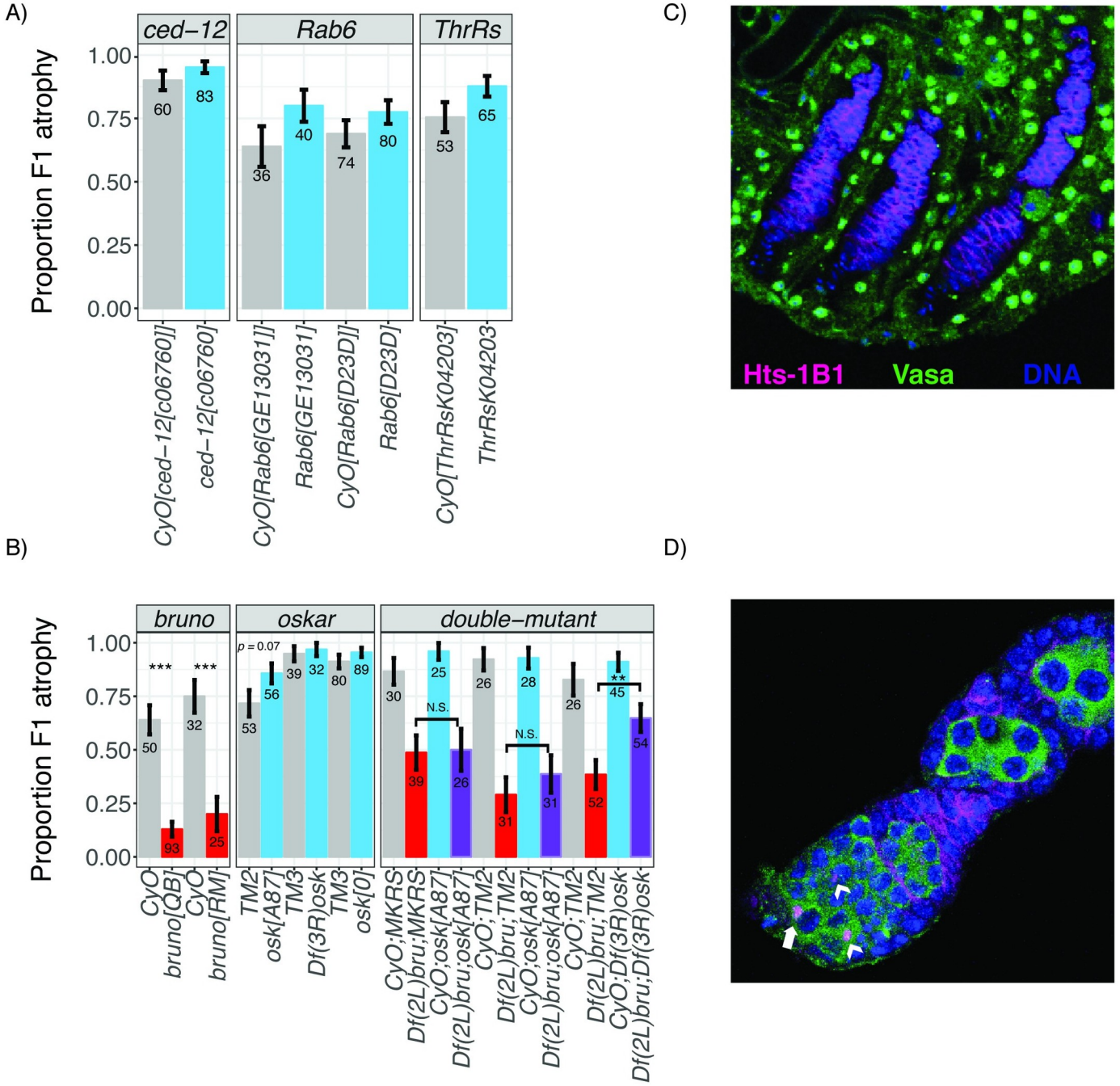

Fig 5. Mutational analysis of candidate genes. (A) Loss-of-function heterozygotes for three candidate genes are compared to their siblings, inheriting the balancer chromosome *CyO* in order to detect zygotic effects on the incidence of ovarian atrophy among 3–7-day-old dysgenic F1 offspring. (B) Single and double loss-of-function and deficiency heterozygotes for *bruno* and *oskar* are compared with their siblings inheriting the balancer chromosomes *CyO* (*bruno*) and *TM2*, *TM3*, or *MKRS* (*oskar*), in order to detect zygotic effects on the incidence of atrophy among 3–7-day-old dysgenic F1 offspring. Offspring from the same cross are represented consecutively on the graph. While *bruno* alleles act as consistent dominant suppressors in both single and double mutants, *oskar* deficiencies and mRNA null mutants exhibit only stochastic effects on the atrophy phenotype, suggesting that the mechanism of *bruno* suppression of F1 atrophy is independent of *oskar* mRNA function. (C-D) Representative germline development among atrophied and non-atrophied ovaries of $bruno^{QB}$/+ and *CyO*/+ dysgenic offspring (B). (C) Atrophied ovaries lack any Vasa-positive germline cells in the ovarioles, including GSCs. Nuclear Vasa external to Hts-1B1 corresponds to the somatic ovarian sheath [35]. (D) Non-atrophied (i.e., morphologically normal) ovaries exhibit the full range of developing oocytes, including GSCs (white arrow). Arrowheads correspond to CBs, the undifferentiated daughters of GSCs. Representative ovaries in both C and D are *CyO*/+; however, atrophied ovaries (C) are more common among $bruno^{QB}$/+ (B). Cytological markers for C and D are hu li tai shao (Hts-1B1), which labels somatic follicle cell membranes, the circular fusomes of GSCs and CBs, and the spectrosomes that connect cells in the developing cyst, and Vasa, which labels the cytoplasm of germline cells and nuclei of the ovarian sheath, and

DAPI staining of nuclear DNA. The individual numerical values required to generate bar plots in panels A and B can be found in S9 and S10 Data, respectively. CB, cystoblast; *CyO*, *Curly-O*; F1, filial 1; GSC, germline stem cell; Hts-1B1, hu li tai shao; *ThrRs*, *Threonyl-tRNA synthetase*; *TM2*, third marked 2; *TM3*, third marked 3.

https://doi.org/10.1371/journal.pbio.2006040.g005

dependency on *oskar* mRNA. While *bruno*'s functions in GSC differentiation are independent of *oskar* mRNA [36,37,56], *bruno* and *oskar*'s impact on vitellogenesis are interdependent, because of the requirement for *oskar* mRNA to sequester Bruno protein [39].

To determine if the effect of *bruno* alleles on hybrid dysgenesis are independent of *oskar* mRNA, we examined whether two *oskar* mRNA null alleles, osk° and osk^{A87}, as well as an *oskar* deficiency, affected the incidence of ovarian atrophy when compared with a balancer control (Fig 5B). We observed that osk° and deficiency on chromosome 3R over *oskar* (*Df(3R)osk*) exhibited no effect on the atrophy phenotype, while osk^{A87} was associated with only a marginal increase in ovarian atrophy ($p = 0.07$). If *bruno* suppression of ovarian atrophy reflects reduced sequestration by *oskar* mRNA in the dysgenic female germline, atrophy should be enhanced by *oskar* mRNA mutants [57].

Comparison of single and double heterozygotes of *bruno* and *oskar* also do not strongly suggest that *bruno* suppression is dependent on *oskar* mRNA dosage (Fig 5B). In comparisons involving two separate balancer third chromosomes, *Df(2L)bru/+; osk*^{A87}/+; double heterozygotes did not differ from their single *Df(2L)bru/+;balancer/+* heterozygous siblings with respect to ovarian atrophy. A second double heterozygote *Df(2L)bru/+;Df(3R)osk/+*; was associated with significantly increased atrophy when compared with the single heterozygote (*Df (2L)bru/+; balancer/+*). However, because this behavior was unique to the deficiency chromosome and was not also exhibited by the osk^{A87} mRNA null mutant that specifically eliminates *oskar* function [38], we suspect it is a synthetic consequence of hemizygosity in both deficiency regions, rather than evidence for a genetic interaction between *oskar* and *bruno*, with respect to hybrid dysgenesis. Consistent with this, we also did not detect any Bruno mislocalization in the developing egg chambers of wild-type dysgenic females (S1 Fig), nor did we see any evidence of an arrest in mid-stage oogenesis in wild-type dysgenic ovaries, as occurs when Bruno is not sequestered by *oskar* mRNA [38,39].

To evaluate whether *bruno* suppression of ovarian atrophy could be explained by its *oskar*-independent role in GSC differentiation [55,58], we directly examined and compared GSCs between $bruno^{QB}$/+ and *CyO*/+ dysgenic ovaries (Fig 5C and 5D). While we did not observe any direct evidence of delayed GSC differentiation in $bruno^{QB}$/+ germaria, we did observe that ovarioles containing developing egg chambers overwhelmingly retained all oogenic stages, including GSCs (Fig 5D). In contrast, atrophied ovaries lacked any developing egg chambers including GSCs (Fig 5C). These observations are consistent with recent evidence that GSC retention is a key determinant of *P*-element–induced ovarian atrophy [35]. They further suggest that reduced *bruno* signaling for differentiation may stabilize GSCs in their niche, allowing them to be retained despite the genotoxic effect of *P*-elements.

Discussion

While the evolution of TE resistance through small-RNA-mediated silencing is a topic of immense research interest, the existence and evolution of tolerance factors that may reduce the fitness costs of TEs on the host remain undocumented. By opportunistically employing a panel of genotyped RILs, which uniformly lack small-RNA-mediated silencing of the recently invaded *P*-element, we have here uncovered the first example of segregating variation in host-TE tolerance in any organism. The natural variation in tolerance that we uncovered is unlikely to be exceptional. Population A RILs were generated from only eight genotypes, sampling but a small subset of alleles that were present in the ancestral population. Furthermore, major QTL

peak that we identified here in Population A explains only about 35% of the heritable variation in tolerance. Therefore, other segregating variants in the Population A RILs must also affect female germline response to *P*-element activity. Our inability to map these variants likely reflects the fact that they are rare, exhibit small effects, or both [30]. Finally, because our phenotyping scheme involved crossing genetically variable RILs to the same paternal strain, zygotic recessive alleles that are not found in the paternal Harwich genotype would remain undetected.

While differences in tolerance may be masked by resistance after small-RNA-mediated silencing evolves, our study reveals that in the absence of silencing, tolerance can be a major determinant of fitness. While the major peak we identified is modest in its functional effects, explaining about 14% of variation in ovarian atrophy, variation in fertility of this scale would be dramatic in the eyes of natural selection. Segregating tolerance alleles, such as the one we have detected here, could therefore be subject to strong positive selection during genome invasion by a novel TE. Tolerance may therefore be an important feature of the host evolutionary response to invading TEs. Indeed, the correlation between *P*-element dosage and the severity of hybrid dysgenesis is poor at best, causing many to suggest that other genetic factors, such as tolerance alleles, may also be important determinants of the dysgenic phenotype [59–61]. Furthermore, the hybrid dysgenesis induced by recent collections of *D. melanogster* tends to be mild when compared to collections from the 1970s and 1980s, providing circumstantial evidence that tolerance factors may have increased in frequency over time [61]. Once the causative variant responsible for the tolerance phenotype we uncovered here is identified, we will be poised to ask whether its increase in frequency has enhanced tolerance in extant populations.

Based on its high expression in the *Drosophila* female ovary [47], the presence of 22 SNPs that are in phase with founder QTL alleles, its differential expression between tolerant and sensitive alleles, and the dominant suppressive effect of classical loss-of-function alleles on dysgenic ovarian atrophy, *bruno* is a very strong candidate for the source of causative variation in *P*-element tolerance that we mapped on chromosome 2L. Identifying the causative variant(s) within the very large (138 kb) *bruno* locus and understanding how its altered function relates to hybrid dysgenesis present exciting challenges for future work. On the surface, it is not obvious how *bruno* function could be related to *P*-element activity. Because Bruno physically interacts with the piRNA pathway component Vasa [62] and localizes to nuage [63], the multifunctional germline organelle in which piRNA biogenesis occurs (reviewed in [64,65]), a straightforward explanation is that *bruno* function is unrelated to tolerance but rather suppresses piRNA-mediated resistance of *P*-elements. However, resistance suppression is inconsistent with several important aspects of piRNA biology and *bruno* function. First, piRNA-mediated silencing of *P*-elements is short-circuited in the absence of complementary maternally deposited piRNAs (absent from the RILs), and *P*-element–derived piRNAs are exceptionally rare in the ovaries of young dysgenic females [42,66]. Thus, the dramatic suppression of ovarian atrophy exhibited by *bruno* alleles in young dysgenic females (Fig 5B) is developmentally inconsistent with piRNA-mediated silencing, which can occur only in older female offspring of dysgenic crosses [42]. Additionally, germline knock-down of *bruno* does not significantly affect TE expression and, if anything, is associated with increased expression of some TE families [67]. If *bruno* suppressed piRNA silencing, reduced TE expression would be predicted upon knock-down.

We propose that our results are best explained by *bruno*'s function in promoting GSC differentiation [37,55], which could determine the tolerance of GSCs to DNA damage resulting from *P*-activity. GSC maintenance is dependent on a balance between self-renewal and differentiation (reviewed in [68]), and is disrupted by the presence of DNA damage, leading to GSC loss [69]. We recently have discovered that the DNA damage response factor p53 is ectopically

activated in the GSCs and CBs of dysgenic germlines [35], which explains why GSCs are frequently absent from dysgenic ovaries (Fig 5C, [15,34,35]). *bruno* loss-of-function alleles could therefore stabilize damaged GSCs in their niche in dysgenic germaria by reducing signals for differentiation. Indeed, loss-of-function mutations in two other GSC differentiation factors, *bag of marbles* and *benign gonial cell neoplasm*, have been associated with enhanced retention of GSCs in the niche of non-dysgenic germaria [70]. This model is fully consistent with our observation that *bruno* suppression of ovarian atrophy is accompanied by a rescue of oogenesis at all stages, including enhanced maintenance of GSCs (Fig 5C).

Our observations with *bruno* suggest an unexpected and novel role for developmental regulators of gametogenesis as determinants of germline tolerance of transposition. Interestingly, multiple regulators of female GSC maintenance and differentiation in *D. melanogaster* exhibit recent or ongoing signatures of positive selection [71–73]. Tolerance to the selfish bacterial endosymbiont *Wolbachia* has already been implicated in driving some of this adaptive evolution [74]. The fact that *bruno* alleles act as strong repressors of *P*-element hybrid dysgenesis suggests that another class of parasites, TEs, may also contribute to the adaptive evolution of stem cell determinants.

Materials and methods

Drosophila strains and husbandry

RILs from Population A were generously provided by Stuart Macdonald. Harwich (#4264), *Ced-12*^{c06760}/*CyO* (#17781), *Rab6*^{GE13031}/*CyO* (#26898), *Rab6*^{D23D}/*CyO* (#5821), and *ThrRS*^{K04203}/*CyO* (#10539) were obtained from the Bloomington *Drosophila* stock center. Harwich was sibmated for one generation to increase homozygosity. *Bruno* and *oskar* mutants and deficiencies, in single and double heterozygous combinations, were generously provided by Paul MacDonald. *Canton-S* was obtained from Richard Meisel. All flies were maintained in standard cornmeal media. All experimental flies were maintained at 25 ˚C.

QTL phenotyping

Virgin RIL females were crossed to Harwich males and flipped onto fresh food every 3–5 days. Resulting F1 offspring were maintained for 3 days or 21 days, at which point their ovaries were examined using a squash prep [60]. Twenty-one-day-old females were transferred onto new food every 5 days as they aged to avoid bacterial growth. For the squash prep, individual females were squashed in a food-dye solution allowed to incubate for $\geq$5 minutes. After incubation, the slide was examined for the presence of stage 14, chorionated egg chambers, which preferentially absorb the dye. In the interest of throughput, we assayed F1 females for the presence or absence of mature egg chambers: females who produced $\geq$1 egg chambers were scored as having non-atrophied ovaries, and females producing 0 egg chambers were scored as having atrophied ovaries. A phenotyping schematic is provided in Fig 1A.

Crosses and phenotyping were performed for 656 RILs across 24 experimental blocks for 3-day-old F1 females and 606 RILs across 21 experimental blocks for 21-day-old F1 females. If fewer than 20 F1 offspring were phenotyped for a given cross, it was discarded and repeated, if possible. In total, we phenotyped $\geq$20 3-day-old and 21-day-old F1 female offspring for 592 RILs and 492 RILs, respectively, and 660 RILs were assayed for at least one of the age groups.

QTL mapping

For age-class-specific QTL mapping (3-day- and 21-day-old), the arcsine transformed proportion of F1 females (S2 Fig) with atrophied ovaries produced by each RIL (S1 and S2 Data) was

used as the response variable in a random effects multiple regression model that included experimental block and undergraduate experimenter.

$$\boldsymbol{asin}\sqrt{atrophy\ proportion} = Block + Experimenter$$

For the combined analysis of both age classes, we used the full set of arcsine transformed proportions, and accounted for female age as an additional fixed effect in the regression model.

$$\boldsymbol{asin}\sqrt{atrophy\ proportion} = Block + Experimenter + Age$$

All models were fit using the lmer function from the lme4 package [75] and are described in S2 Table.

The raw residuals of the regression models above were used as the phenotypic response for QTL analysis (S3–S5 Data), implemented with the DSPRqtl package [29] in R 3.02 [76]. The output yields a LOD score for the observed association between phenotype and genotype at 11,768 10-kb intervals along the euchromatic arms of the X, second, and third chromosomes. The LOD significance threshold was determined from 1,000 permutations of the observed data, and the confidence interval around each LOD peak was identified by a difference of −2 from the LOD peak position (Δ2-LOD), as well as a Bayesian credible interval [44].

Broad sense heritability

Maternal genotype was added as a random effect to the models above, in order to determine the genetic variance in the phenotype (V^G). V^G was obtained by extracting the variance component for maternal genotype using the VarCorr() function from the nlme package [77]. Broad sense heritability (H^2) was then the estimated proportion of overall variance (V^G/V^P).

Estimation of founder phenotypes and QTL phasing

To estimate the phenotypic effect of each founder at the QTL peak, we considered the residual phenotype for each used in QTL mapping and then determined the founder allele carried by the RIL at the LOD peak position [29]. RILs whose genotype at the LOD peak could not be assigned to a single founder with >0.95 probability were discarded.

Founder alleles were phased into phenotypic classes by identifying the minimal number of groups required to describe phenotypic variation associated with the QTL peak [29]. Briefly, founder alleles were sorted based on their average estimated phenotypic effect, which was provided by the sampled RILs. Linear models containing all possible sequential partitions of founder alleles were then fit and compared to a null model in which all founder alleles are in a single partition, using an extra-sum-of-squares *F*-test. The two-partition model with the highest *F*-statistic was retained and fixed only if it provided a significantly better fit ($p < 10^{-4}$) than the null model. The two partitions of founder haplotypes were then fixed, and all possible three-partition models were explored. This process was continued until the model fit could not be improved.

Identification of in-phase polymorphisms and TEs

Founders were assigned a "hard" genotype for all annotated TEs [78] and SNPs [29] in the QTL window if their genotype probability for a given allele was greater than 0.95 [29]. We then looked for alternate alleles (SNPs and TEs) that were in phase with our inferred allelic classes [29,31]: the sensitive class (A3 and A5) and the tolerant class (A1, A2, A4, A6, and A7).

A8 was excluded because its assignment to the sensitive or tolerant class differed between the data sets from 3-day-old and 21-day-old females.

Identification of background-matched, sensitive, and tolerant RIL pairs

To identify RILs containing either the A4 ("tolerant") or A5 ("sensitive") haplotypes for the QTL window, we took advantage of the published, hidden Markov model–inferred genotypes for the Population A RIL panel [29]. We first identified RILs that carried a contiguous A4 or A5 haplotype for the Δ2-LOD confidence interval for the combined analysis with a genotype probability of greater than 0.95 (Table 1). Then, for all possible RIL pairs (A4 and A5), we calculated the number of 10-kb genomic windows for which they carried the same RIL haplotype, also with a genotype probability of greater than 0.95. We selected three pairs of background-matched RILs, which carry the same founder haplotype for 67% (11374 and 11120), 64% (11131 and 11200), and 60% (11435 and 11343) of genomic windows but alternate haplotypes for the QTL window.

F1 fertility

Virgin female offspring of dysgenic crosses between tolerant (11120, 11200, 11343) and sensitive (11374, 11131, 11435) RILs and Harwich males were collected daily and placed individually in a vial with two *ywF10* males. Females were allowed to mate and oviposit for 5 days, and adults were discarded when the females reached 6 days of age. The presence and number of F2 offspring were quantified for each dysgenic female. The effects of genetic background and QTL haplotype on the presence and number of F1 offspring were assessed by logistic and linear regression models, respectively. Models were fit using the glm (logistic) and lm (linear) functions in R 3.02 [76].

Quantitative PCR

Ovaries were dissected from young, 3-day-old females from tolerant (11120, 11200, 11343) and sensitive (11374, 11131, 11435) RILs and homogenized in TRI-reagent (Sigma-Aldrich). RNA was extracted according to manufacturer instructions. Purified RNA was treated with DNAse, reverse transcribed using oligo$(dT)_{15}$ primers and M-MLV RNAseH–, and then treated with RNAse H, according to manufacturer instructions (Promega). Synthesized cDNA was diluted 1:125 for qRT-PCR.

Abundance of *bruno* and *rpl32* transcript was estimated using SYBR green PCR mastermix (Applied Biosystems) according to manufacturer instructions. Three biological replicates were evaluated for each genotype, with three technical measurements for each replicate, for a total of nine measurements of each genotype. *Bruno* expression was estimated relative to *rpl32* for each replicate, according to a five-point standard curve. Primers were as follows: *bruno*-F: 5′-CCCAGGATGCTTTGCATAAT-3′, *bruno*-R: 5′- ACGTCGTTCTCGTTCAGCTT-3′, *rpl32*-F: CCGCTTCAAGGGACAGTATC, and *rpl32*-F: GACAATCTCCTTGCGCTTCT. The relationship between genetic background and QTL haplotype with *bruno* expression was evaluated with mixed-effects linear regression, accounting for the biological replicate as a random effect. The regression model was fit with the lme4 package [75] in R 3.02 [76].

Mutational analysis of candidate genes

Single and double heterozygote mutant virgin females (*mutant/balancer*) were crossed to Harwich males at 25 ˚C. Because the vast majority of *Drosophila* lab stocks are *P*-element–free, with the exception of any *P*-element–derived transgenes, these crosses are dysgenic. Resulting

F1 dysgenic female offspring were collected and aged at 25 ˚C for 3–7 days, when their ovaries were assayed using the squash prep described above [60]. The incidence of ovarian atrophy was then compared between *mutant*/+ and *balancer*/+ siblings from the same cross.

Immunolabelling

Ovaries from 3–7-day-old female offspring of dysgenic crosses were dissected and immediately fixed with 4% EM-grade methanol-free paraformaldehyde (Thermo Scientific). Ovaries were washed with 0.1% Triton X-100 in PBS and blocked with 5% goat serum albumin (Sigma-Aldrich). Primary antibody concentrations were as follows: anti-Hts 1B1 1:4 (DSHB [79]), anti-Vasa 1:40 (DSHB), anti-Bruno 1:1,000 (provided by Paul MacDonald [50]), and anti-Orb 4H8 and 6H4 1:20 (DSHB [50]). Secondary antibody concentrations were 1:500.

Microscopy

Ovaries were visualized with an SP8 Upright Confocal DM6000 CFS (Leica) Microscope, outfitted with a 60× oil immersion lens. Images were collected using an EM-CCD camera (Hamamatsu) and LAS-AF software (Leica).

Supporting information

S1 Data. Proportion atrophy for 3-day-old F1 females. For each sampled RIL, the strain number (matRIL), experimental block, student experimenter, and proportion atrophy are provided. F1, filial 1; matRIL, maternal recombinant inbred line; RIL, recombinant inbred line.
(XLSX)

S2 Data. Proportion atrophy for 21-day-old F1 females. For each sampled RIL, the strain number (matRIL), experimental block, student experimenter, and proportion atrophy are provided. F1, filial 1; matRIL, maternal recombinant inbred line; RIL, recombinant inbred line.
(XLSX)

S3 Data. Residuals from combined regression, including both 3-day-old and 21-day-old females, used for QTL mapping. For each sampled RIL, the strain number (matRIL), experimental block, student experimenter, and residual are provided. matRIL, maternal recombinant inbred line; QTL, quantitative trait locus; RIL, recombinant inbred line.
(XLSX)

S4 Data. Residuals from 3-day-old females used for QTL mapping. For each sampled RIL, the strain number (matRIL), experimental block, student experimenter, and residual are provided. matRIL, maternal recombinant inbred line; QTL, quantitative trait locus; RIL, recombinant inbred line.
(XLSX)

S5 Data. Residuals from 21-day-old females used for QTL mapping. For each sampled RIL, the strain number (matRIL), experimental block, student experimenter, and residual are provided. matRIL, maternal recombinant inbred line; QTL, quantitative trait locus; RIL, recombinant inbred line.
(XLSX)

S6 Data. Ovarian atrophy among dysgenic F1 offspring of background-matched RILs. An atrophy score of 1 denotes atrophied ovaries, while 0 indicates non-atrophied ovaries. For each female, the maternal RIL, background, and phenotype are provided. F1, filial 1; RIL,

recombinant inbred line.
(XLSX)

S7 Data. Fertility among dysgenic F1 offspring of background-matched RILs. For each female, the number of F2 offspring produced, the maternal RIL, background, and phenotype are provided. F1, filial 1; F2, filial 2; RIL, recombinant inbred line.
(XLSX)

S8 Data. Bruno expression in background-matched RILs. *bruno* expression levels (relative to *rpl32*), RIL genotype, background, phenotype, and biological replicate are provided. RIL, recombinant inbred line.
(XLSX)

S9 Data. Ovarian atrophy among F1 dysgenic offspring of candidate gene heterozygous mutant mothers. The raw counts and proportion of atrophied and non-atrophied ovaries are provided for different offspring classes. Genotype indicates the zygotic genotype. Gene indicates gene affected by a heterozygous loss-of-function allele in the maternal genotype. Allele indicates the specific loss-of-function mutation. F1, filial 1.
(XLSX)

S10 Data. Ovarian atrophy among F1 dysgenic offspring of *bruno* and *oskar* mutant mothers. The raw counts and proportion of atrophied and non-atrophied ovaries are provided for different offspring classes. Genotype indicates the zygotic genotype. Gene indicates whether the maternal genotype was heterozygous for a *bruno* loss-of-function allele, an *oskar* loss-of-function allele, or both. Allele indicates which mutations were found in the maternal genotype. F1, filial 1.
(XLSX)

S1 Table. In-phase polymorphisms within the QTL peak. The chromosomal position on autosome 2L is provided for 36 in-phase polymorphic SNPs. Coordinates are based on release 6 of the *Drosophila melanogaster* genome [45]. The allele found in the founder genome is specified as ref or alt (A1–A8). Putative effects on annotated genes are indicated according to the UCSC Genome Browser annotations [46]. ALT, indicates the nucleotide at this position found in the alternative allele; QTL, quantitative trait locus; REF, indicates the nucleotide at this position found in the reference genome; SNP, single nucleotide polymorphism; UCSC, University of California at Santa Cruz.
(XLSX)

S2 Table. Random-effects ANOVA results for 3-day-old F1 females, 21-day-old F1 females, and a combined analysis including both age classes. F1, filial 1.
(XLSX)

S1 Fig. Bruno localization does not differ between dysgenic and non-dysgenic ovaries. Bruno localization in mid-stage (4–6) oocytes of non-dysgenic (A) and dysgenic (B) females from reciprocal crosses between Canton-S and Harwich. In both genotypes, Bruno protein forms cytoplasmic, perinuclear rings.
(TIF)

S2 Fig. Arcsine transformed and untransformed proportions of F1 atrophy among 3-day-old and 21-day-old females. Individual data points required to generate histograms are provided in S4 and S5 Data. F1, filial 1.
(TIF)

Acknowledgments

We are grateful to Stuart Macdonald, Paul MacDonald, and Richard Meisel for *Drosophila* strains and Paul MacDonald for anti-Bruno antibodies. Ryan Castelluci, Ashka Shah, and Wesley Adalume assisted in phenotyping atrophy among F1 offspring. Stuart Macdonald and Daniel Barbash provided helpful discussion and feedback on this manuscript.

Author Contributions

Conceptualization: Erin S. Kelleher.

Data curation: Erin S. Kelleher, Jaweria Jaweria, Uchechukwu Akoma, Lily Ortega, Wenpei Tang.

Formal analysis: Erin S. Kelleher.

Funding acquisition: Erin S. Kelleher.

Investigation: Erin S. Kelleher, Jaweria Jaweria, Uchechukwu Akoma, Lily Ortega, Wenpei Tang.

Methodology: Erin S. Kelleher.

Project administration: Erin S. Kelleher.

Supervision: Erin S. Kelleher.

Validation: Erin S. Kelleher.

Visualization: Erin S. Kelleher.

Writing – original draft: Erin S. Kelleher.

Writing – review & editing: Erin S. Kelleher.

References

1. Chénais B, Caruso A, Hiard S, Casse N. The impact of transposable elements on eukaryotic genomes: from genome size increase to genetic adaptation to stressful environments. Gene. 2012; 509: 7–15. https://doi.org/10.1016/j.gene.2012.07.042 PMID: 22921893
2. Vitte C, Panaud O. LTR retrotransposons and flowering plant genome size: emergence of the increase/decrease model. Cytogenet Genome Res. Karger Publishers; 2005; 110: 91–107. https://doi.org/10.1159/000084941 PMID: 16093661
3. Sun C, Shepard DB, Chong RA, López Arriaza J, Hall K, Castoe TA, et al. LTR retrotransposons contribute to genomic gigantism in plethodontid salamanders. Genome Biol Evol. 2012; 4: 168–83. https://doi.org/10.1093/gbe/evr139 PMID: 22200636
4. Kunarso G, Chia N-Y, Jeyakani J, Hwang C, Lu X, Chan Y-S, et al. Transposable elements have rewired the core regulatory network of human embryonic stem cells. Nat Genet. 2010; 42: 631–4. https://doi.org/10.1038/ng.600 PMID: 20526341
5. Lynch VJ, Leclerc RD, May G, Wagner GP. Transposon-mediated rewiring of gene regulatory networks contributed to the evolution of pregnancy in mammals. Nat Genet. 2011; 43: 1154–9. https://doi.org/10.1038/ng.917 PMID: 21946353
6. Startek M, Szafranski P, Gambin T, Campbell IM, Hixson P, Shaw CA, et al. Genome-wide analyses of LINE-LINE-mediated nonallelic homologous recombination. Nucleic Acids Res. 2015; https://doi.org/10.1093/nar/gku1394 PMID: 25613453
7. Rajaei N, Chiruvella KK, Lin F, Astrom SU. Domesticated transposase Kat1 and its fossil imprints induce sexual differentiation in yeast. Proc Natl Acad Sci. 2014; 111: 15491–15496. https://doi.org/10.1073/pnas.1406027111 PMID: 25313032
8. Kapitonov VV, Jurka J. RAG1 Core and V(D)J Recombination Signal Sequences Were Derived from Transib Transposons. Nemazee D, editor. PLoS Biol. Public Library of Science; 2005; 3: e181. https://doi.org/10.1371/journal.pbio.0030181 PMID: 15898832

9. Silva-Sousa R, López-Panadès E, Casacuberta E. Drosophila telomeres: an example of co-evolution with transposable elements. Genome Dyn. 2012; 7: 46–67. https://doi.org/10.1159/000337127 PMID: 22759813
10. Aminetzach YT, Macpherson JM, Petrov DA. Pesticide resistance via transposition-mediated adaptive gene truncation in Drosophila. Science. 2005; 309: 764–7. https://doi.org/10.1126/science.1112699 PMID: 16051794
11. Mateo L, Ullastres A, González J. A Transposable Element Insertion Confers Xenobiotic Resistance in Drosophila. Feschotte C, editor. PLoS Genet. 2014; 10: e1004560. https://doi.org/10.1371/journal.pgen.1004560 PMID: 25122208
12. van't Hof AE, Campagne P, Rigden DJ, Yung CJ, Lingley J, Quail MA, et al. The industrial melanism mutation in British peppered moths is a transposable element. Nature. Nature Research; 2016; 534: 102–105. https://doi.org/10.1038/nature17951 PMID: 27251284
13. Dupuy AJ, Fritz S, Largaespada DA. Transposition and gene disruption in the male germline of the mouse. Genesis. 2001; 30: 82–8 [cited 2015 Oct 15]. Available from: http://www.ncbi.nlm.nih.gov/pubmed/11416868 PMID: 11416868
14. Spradling AC, Stern D, Beaton A, Rhem EJ, Laverty T, Mozden N, et al. The Berkeley Drosophila Genome Project gene disruption project: Single P-element insertions mutating 25% of vital Drosophila genes. Genetics. 1999; 153: 135–77 [cited 2015 Feb 17]. Available from: http://www.pubmedcentral.nih.gov/articlerender.fcgi?artid=1460730&tool=pmcentrez&rendertype=abstract PMID: 10471706
15. Dorogova N V., Bolobolova EU, Zakharenko LP. Cellular aspects of gonadal atrophy in Drosophila P-M hybrid dysgenesis. Dev Biol. 2017; 424: 105–112. https://doi.org/10.1016/j.ydbio.2017.02.020 PMID: 28283407
16. Noutsopoulos D, Markopoulos G, Vartholomatos G, Kolettas E, Kolaitis N, Tzavaras T. VL30 retrotransposition signals activation of a caspase-independent and p53-dependent death pathway associated with mitochondrial and lysosomal damage. Cell Res. 2010; 20: 553–562. https://doi.org/10.1038/cr.2010.48 PMID: 20386572
17. Roy BA, Kirchner JW. Evolutionary dynamics of pathogen resistance and tolerance. Evolution. 2000; 54: 51–63 [cited 2018 Feb 22]. Available from: http://www.ncbi.nlm.nih.gov/pubmed/10937183 PMID: 10937183
18. Mauricio R. Natural selection and the joint evolution of toleranceand resistance as plant defenses. Evol Ecol. Kluwer Academic Publishers; 2000; 14: 491–507. https://doi.org/10.1023/A:1010909829269
19. Blumenstiel JP. Evolutionary dynamics of transposable elements in a small RNA world. Trends Genet. Elsevier Ltd; 2011; 27: 23–31. https://doi.org/10.1016/j.tig.2010.10.003 PMID: 21074888
20. Yang P, Wang Y, Macfarlan TS. The Role of KRAB-ZFPs in Transposable Element Repression and Mammalian Evolution. Trends Genet. 2017; https://doi.org/10.1016/j.tig.2017.08.006 PMID: 28935117
21. Senti K-A, Brennecke J. The piRNA pathway: a fly's perspective on the guardian of the genome. Trends Genet. 2010; 26: 499–509. https://doi.org/10.1016/j.tig.2010.08.007 PMID: 20934772
22. Aravin AA, Hannon GJ, Brennecke J. The Piwi-piRNA pathway provides an adaptive defense in the transposon arms race. Science. 2007; 318: 761–4. https://doi.org/10.1126/science.1146484 PMID: 17975059
23. Schaack S, Gilbert C, Feschotte C. Promiscuous DNA: Horizontal transfer of transposable elements and why it matters for eukaryotic evolution. Trends Ecol Evol. 2010; 25: 537–546. https://doi.org/10.1016/j.tree.2010.06.001 PMID: 20591532
24. Kelleher ES. Reexamining the P-Element Invasion of Drosophila melanogaster Through the Lens of piRNA Silencing. Genetics. 2016; 203: 1513–31. https://doi.org/10.1534/genetics.115.184119 PMID: 27516614
25. Kofler R, Hill T, Nolte V, Betancourt AJ, Schlötterer C. The recent invasion of natural Drosophila simulans populations by the P-element. Proc Natl Acad Sci. 2015; 112: 201500758. https://doi.org/10.1073/pnas.1500758112 PMID: 25964349
26. Hill T, Schlötterer C, Betancourt AJ. Hybrid Dysgenesis in Drosophila simulans Associated with a Rapid Invasion of the P-Element. PLoS Genet. 2016; 12: e1005920. https://doi.org/10.1371/journal.pgen.1005920 PMID: 26982327
27. Kidwell MG. Evolution of hybrid dysgenesis determinants in Drosophila melanogaster. Proc Natl Acad Sci U S A. 1983; 80: 1655–9 [cited 2013 Dec 13]. Available from: http://www.pubmedcentral.nih.gov/articlerender.fcgi?artid=393661&tool=pmcentrez&rendertype=abstract PMID: 6300863
28. Kidwell MG, Frydrk T, Novy J. The hybrid dysgenesis potential of Drosophila melanogaster from diverse temporal and geographic origins. Drosoph Inf Serv. 1983; 59: 63–69.

29. King EG, Merkes CM, McNeil CL, Hoofer SR, Sen S, Broman KW, et al. Genetic dissection of a model complex trait using the Drosophila Synthetic Population Resource. Genome Res. 2012; 22: 1558–66. https://doi.org/10.1101/gr.134031.111 PMID: 22496517

30. King EG, Macdonald SJ, Long AD. Properties and power of the Drosophila Synthetic Population Resource for the routine dissection of complex traits. Genetics. 2012; 191: 935–49. https://doi.org/10.1534/genetics.112.138537 PMID: 22505626

31. Long AD, Macdonald SJ, King EG. Dissecting complex traits using the Drosophila Synthetic Population Resource. Trends Genet. 2014; 30: 488–495. https://doi.org/10.1016/j.tig.2014.07.009 PMID: 25175100

32. Bucheton A. I transposable elements and I-R hybrid dysgenesis in Drosophila. Trends Genet. 1990; 6: 16–21 [cited 2018 Feb 22]. Available from: http://www.ncbi.nlm.nih.gov/pubmed/2158161 PMID: 2158161

33. Malone CD, Lehmann R, Teixeira FK. The cellular basis of hybrid dysgenesis and Stellate regulation in Drosophila. Curr Opin Genet Dev. 2015; 34: 88–94. https://doi.org/10.1016/j.gde.2015.09.003 PMID: 26451497

34. Schaefer RE, Kidwell MG, Fausto-Sterling A. Hybrid Dysgenesis in Drosophila melanogaster: Morphological and Cytological Studies of Ovarian Dysgenesis. Genetics. 1979; 92: 1141–52 [cited 2012 June 4]. Available from: http://www.pubmedcentral.nih.gov/articlerender.fcgi?artid=1214061&tool=pmcentrez&rendertype=abstract PMID: 17248944

35. Tasnim S, Kelleher ES. p53 is required for female germline stem cell maintenance in P- element hybrid dysgenesis. Dev Biol. 2018; 434: 215–220. https://doi.org/10.1016/j.ydbio.2017.12.021 PMID: 29294306

36. Kim-Ha J, Kerr K, Macdonald PM. Translational regulation of oskar mRNA by bruno, an ovarian RNA-binding protein, is essential. Cell. 1995; 81: 403–12 [cited 2018 Feb 20]. Available from: http://www.ncbi.nlm.nih.gov/pubmed/7736592 PMID: 7736592

37. Wang Z, Lin H. Sex-lethal is a target of Bruno-mediated translational repression in promoting the differentiation of stem cell progeny during Drosophila oogenesis. Dev Biol. 2007; 302: 160–168. https://doi.org/10.1016/j.ydbio.2006.09.016 PMID: 17067567

38. Jenny A, Hachet O, Závorszky P, Cyrklaff A, Weston MDJ, Johnston DS, et al. A translation-independent role of oskar RNA in early Drosophila oogenesis. Development. 2006; 133 [cited 2017 July 15]. Available from: http://dev.biologists.org/content/133/15/2827

39. Kanke M, Jambor H, Reich J, Marches B, Gstir R, Ryu YH, et al. oskar RNA plays multiple noncoding roles to support oogenesis and maintain integrity of the germline/soma distinction. RNA. 2015; 21: 1096–109. https://doi.org/10.1261/rna.048298.114 PMID: 25862242

40. Kidwell MG, Kidwell JF, Sved JA. Hybrid Dysgenesis in Drosophila melanogaster: A Syndrome of Aberrant Traits Including Mutation, Sterility and Male Recombination. Genetics. 1977; 86: 813–33 [cited 2014 Sept 16]. Available from: http://www.pubmedcentral.nih.gov/articlerender.fcgi?artid=1213713&tool=pmcentrez&rendertype=abstract PMID: 17248751

41. Engels WR, Preston CR. Hybrid dysgenesis in Drosophila melanogaster: the biology of female and male sterility. Genetics. 1979; 92: 161–74 [cited 2016 Feb 25]. Available from: http://www.pubmedcentral.nih.gov/articlerender.fcgi?artid=1213938&tool=pmcentrez&rendertype=abstract PMID: 115745

42. Khurana JS, Wang J, Xu J, Koppetsch BS, Thomson TC, Nowosielska A, et al. Adaptation to P element transposon invasion in Drosophila melanogaster. Cell. 2011; 147: 1551–63. https://doi.org/10.1016/j.cell.2011.11.042 PMID: 22196730

43. Hartmann MA, Sekelsky J. The absence of crossovers on chromosome *4* in *Drosophila melanogaster*: Imperfection or interesting exception? Fly (Austin). Taylor & Francis; 2017; 11: 253–259. https://doi.org/10.1080/19336934.2017.1321181

44. Manichaikul A, Dupuis J, Sen S, Broman KW. Poor performance of bootstrap confidence intervals for the location of a quantitative trait locus. Genetics. Genetics Society of America; 2006; 174: 481–9. https://doi.org/10.1534/genetics.106.061549 PMID: 16783000

45. Hoskins RA, Carlson JW, Wan KH, Park S, Mendez I, Galle SE, et al. The Release 6 reference sequence of the Drosophila melanogaster genome. Genome Res. 2015; 25: 445–58. https://doi.org/10.1101/gr.185579.114 PMID: 25589440

46. Casper J, Zweig AS, Villarreal C, Tyner C, Speir ML, Rosenbloom KR, et al. OUP accepted manuscript. Nucleic Acids Res. 2017; 46: D762–D769.

47. Brown JB, Boley N, Eisman R, May GE, Stoiber MH, Duff MO, et al. Diversity and dynamics of the Drosophila transcriptome. Nature. 2014; 512: 393–399. https://doi.org/10.1038/nature12962 PMID: 24670639

48. King EG, Long AD. The Beavis Effect in Next-Generation Mapping Panels in Drosophila melanogaster. G3 (Bethesda). Genetics Society of America; 2017; 7: 1643–1652. PMID: 28592647

49. Schüpbach T, Wieschaus E. Female sterile mutations on the second chromosome of Drosophila melanogaster. II. Mutations blocking oogenesis or altering egg morphology. Genetics. 1991; 129: 1119–36 [cited 2018 Oct 9]. Available from: http://www.ncbi.nlm.nih.gov/pubmed/1783295 PMID: 1783295

50. Filardo P, Ephrussi A. Bruno regulates gurken during Drosophila oogenesis. Mech Dev. 2003; 120: 289–97 [cited 2017 July 18]. Available from: http://www.ncbi.nlm.nih.gov/pubmed/12591598 PMID: 12591598

51. Nilton A, Oshima K, Zare F, Byri S, Nannmark U, Nyberg KG, et al. Crooked, Coiled and Crimpled are three Ly6-like proteins required for proper localization of septate junction components. Development. 2010; 137: 2427–2437. https://doi.org/10.1242/dev.052605 PMID: 20570942

52. Chakraborty M, VanKuren NW, Zhao R, Zhang X, Kalsow S, Emerson JJ. Hidden genetic variation shapes the structure of functional elements in Drosophila. Nat Genet. Nature Publishing Group; 2018; 50: 20–25. https://doi.org/10.1038/s41588-017-0010-y PMID: 29255259

53. Thibault ST, Singer MA, Miyazaki WY, Milash B, Dompe NA, Singh CM, et al. A complementary transposon tool kit for Drosophila melanogaster using P and piggyBac. Nat Genet. 2004; 36: 283–287. https://doi.org/10.1038/ng1314 PMID: 14981521

54. Parks AL, Cook KR, Belvin M, Dompe NA, Fawcett R, Huppert K, et al. Systematic generation of high-resolution deletion coverage of the Drosophila melanogaster genome. Nat Genet. 2004; 36: 288–92. https://doi.org/10.1038/ng1312 PMID: 14981519

55. Parisi MJ, Deng W, Wang Z, Lin H. The arrest gene is required for germline cyst formation during Drosophila oogenesis. Genesis. 2001; 29: 196–209 [cited 2017 June 25]. Available from: http://www.ncbi.nlm.nih.gov/pubmed/11309853 PMID: 11309853

56. Kim-Ha J, Smith JL, Macdonald PM. oskar mRNA is localized to the posterior pole of the Drosophila oocyte. Cell. 1991; 66: 23–35 [cited 2018 Feb 20]. Available from: http://www.ncbi.nlm.nih.gov/pubmed/2070416 PMID: 2070416

57. Lander ES, Linton LM, Birren B, Nusbaum C, Zody MC, Baldwin J, et al. Initial sequencing and analysis of the human genome. Nature. 2001; 409: 860–921. https://doi.org/10.1038/35057062 PMID: 11237011

58. Xin T, Xuan T, Tan J, Li M, Zhao G, Li M. The Drosophila putative histone acetyltransferase Enok maintains female germline stem cells through regulating Bruno and the niche. Dev Biol. 2013; 384: 1–12. https://doi.org/10.1016/j.ydbio.2013.10.001 PMID: 24120347

59. Bergman CM, Han S, Nelson MG, Bondarenko V, Kozeretska I. Genomic analysis of *P* elements in natural populations of *Drosophila melanogaster*. PeerJ. PeerJ Inc.; 2017; 5: e3824. https://doi.org/10.7717/peerj.3824 PMID: 28929030

60. Srivastav SP, Kelleher ES. Paternal Induction of Hybrid Dysgenesis in Drosophila melanogaster Is Weakly Correlated with Both P -Element and hobo Element Dosage. G3: Genes|Genomes|Genetics. 2017; g3.117.040634.

61. Ignatenko OM, Zakharenko LP, Dorogova N V, Fedorova SA. P elements and the determinants of hybrid dysgenesis have different dynamics of propagation in Drosophila melanogaster populations. Genetica. 2015; 143: 751–9. https://doi.org/10.1007/s10709-015-9872-z PMID: 26530414

62. Webster PJ, Liang L, Berg CA, Lasko P, Macdonald PM. Translational repressor bruno plays multiple roles in development and is widely conserved. Genes Dev. Cold Spring Harbor Laboratory Press; 1997; 11: 2510–21 [cited 2018 June 12]. Available from: http://www.ncbi.nlm.nih.gov/pubmed/9334316

63. Snee MJ, Macdonald PM. Live imaging of nuage and polar granules: evidence against a precursor-product relationship and a novel role for Oskar in stabilization of polar granule components. J Cell Sci. 2004; 117: 2109–20. https://doi.org/10.1242/jcs.01059 PMID: 15090597

64. Kloc M, Jedrzejowska I, Tworzydlo W, Bilinski SM. Balbiani body, nuage and sponge bodies–The germ plasm pathway players. Arthropod Struct Dev. 2014; 43: 341–348. https://doi.org/10.1016/j.asd.2013.12.003 PMID: 24398038

65. Lehmann R. Germ Plasm Biogenesis—An Oskar-Centric Perspective. Current topics in developmental biology. 2016. pp. 679–707. https://doi.org/10.1016/bs.ctdb.2015.11.024 PMID: 26970648

66. Brennecke J, Malone CD, Aravin AA, Sachidanandam R, Stark A, Hannon GJ. An epigenetic role for maternally inherited piRNAs in transposon silencing. Science. 2008; 322: 1387–92. https://doi.org/10.1126/science.1165171 PMID: 19039138

67. Czech B, Preall JB, McGinn J, Hannon GJ. A transcriptome-wide RNAi screen in the Drosophila ovary reveals factors of the germline piRNA pathway. Mol Cell. NIH Public Access; 2013; 50: 749–61. https://doi.org/10.1016/j.molcel.2013.04.007 PMID: 23665227

68. Sherman MH, Bassing CH, Teitell MA. Regulation of cell differentiation by the DNA damage response. Trends Cell Biol. NIH Public Access; 2011; 21: 312–9. https://doi.org/10.1016/j.tcb.2011.01.004 PMID: 21354798

69. Ma X, Han Y, Song X, Do T, Yang Z, Ni J, et al. DNA damage-induced Lok/CHK2 activation compromises germline stem cell self-renewal and lineage differentiation. Development. 2016; 143: 4312–4323. https://doi.org/10.1242/dev.141069 PMID: 27729408

70. Jin Z, Kirilly D, Weng C, Kawase E, Song X, Smith S, et al. Differentiation-Defective Stem Cells Outcompete Normal Stem Cells for Niche Occupancy in the Drosophila Ovary. Cell Stem Cell. 2008; 2: 39–49. https://doi.org/10.1016/j.stem.2007.10.021 PMID: 18371420

71. Civetta A, Rajakumar SA, Brouwers B, Bacik JP. Rapid evolution and gene-specific patterns of selection for three genes of spermatogenesis in Drosophila. Mol Biol Evol. 2006; 23: 655–62. https://doi.org/10.1093/molbev/msj074 PMID: 16357040

72. Bauer DuMont VL, Flores HA, Wright MH, Aquadro CF. Recurrent positive selection at bgcn, a key determinant of germ line differentiation, does not appear to be driven by simple coevolution with its partner protein bam. Mol Biol Evol. 2007; 24: 182–91. https://doi.org/10.1093/molbev/msl141 PMID: 17056645

73. Flores HA, DuMont VLB, Fatoo A, Hubbard D, Hijji M, Barbash DA, et al. Adaptive Evolution of Genes Involved in the Regulation of Germline Stem Cells in *Drosophila melanogaster* and *D. simulans*. G3: Genes|Genomes|Genetics. 2015; 5: 583–592. https://doi.org/10.1534/g3.114.015875 PMID: 25670770

74. Flores HA, Bubnell JE, Aquadro CF, Barbash DA. The Drosophila bag of marbles Gene Interacts Genetically with Wolbachia and Shows Female-Specific Effects of Divergence. Malik HS, editor. PLOS Genet. 2015; 11: e1005453. https://doi.org/10.1371/journal.pgen.1005453 PMID: 26291077

75. Bates D, Mächler M, Bolker B, Walker S. Fitting Linear Mixed-Effects Models Using lme4. J Stat Softw. 2015; 67: 1–48. https://doi.org/10.18637/jss.v067.i01

76. R Development Core Team. R: A Language and Environment for Statistical Computing [Internet]. Vienna, Austria; 2008 [cited 2018 Oct 9]. http://www.r-project.org

77. Pinheiro J, Bates D, DebRoy S, Sarkar D, R Core Team. {nlme}: Linear and Nonlinear Mixed Effects Models [Internet]. 2016 [cited 2018 Oct 9]. http://cran.r-project.org/package=nlme

78. Cridland JM, Macdonald SJ, Long AD, Thornton KR. Abundance and distribution of transposable elements in two Drosophila QTL mapping resources. Mol Biol Evol. 2013; 30: 2311–27. https://doi.org/10.1093/molbev/mst129 PMID: 23883524

79. Zaccai M, Lipshitz HD. Role ofAdducin-like (hu-li tai shao) mRNA and protein localization in regulating cytoskeletal structure and function duringDrosophila oogenesis and early embryogenesis. Dev Genet. 1996; 19: 249–257. https://doi.org/10.1002/(SICI)1520-6408(1996)19:3<249::AID-DVG8>3.0.CO;2-9 PMID: 8952067